Applied Geochemistry 97 (2018) 270–278

Contents lists available at ScienceDirect

Applied Geochemistry

journal homepage: www.elsevier.com/locate/apgeochem

On the fate of oxygen in a spent fuel emplacement drift in Opalinus Clay

N. Giroud[a,*], Y. Tomonaga[b], P. Wersin[b], S. Briggs[c], F. King[d], T. Vogt[a], N. Diomidis[a]

[a] Nagra, National Cooperative for the Disposal of Radioactive Waste, Wettingen, CH-5430, Switzerland
[b] Institute of Geological Sciences, University of Bern, Bern, CH-3012, Switzerland
[c] Dynamic Consulting, Uxbridge, ON, L9P 1Z3, Canada
[d] Integrity Corrosion Consulting Ltd., Nanaimo, BC, V9T 1K2, Canada

A B S T R A C T

Persistence of aerobic conditions after backfilling of a spent fuel emplacement drift is of high relevance for the selection of canister material and canister design, as well as for the prediction of the onset of H_2 production. This paper presents the results of the O_2 monitoring during the backfilling and early heating phases of the Full-scale Emplacement Experiment at the Mont Terri underground laboratory (Switzerland), as well as the first results of laboratory experiments and 3D reactive transport modelling which aim at identifying the processes controlling O_2 concentrations. The monitoring shows the disappearance of gaseous O_2 and onset of anaerobic corrosion in sections not affected by O_2 inflow from the access tunnel within weeks after backfilling, and even before closure of the drift for the deepest parts of the experiment. The laboratory experiments show that O_2 can significantly adsorb on granular bentonite exposed to high temperatures and might in principle also adsorb at ambient temperature and relative humidity as low as 55%. Thus, gas sorption should be considered in the balance of O_2 in the experiment. These results are consistent with the numerical model indicating that the excavation damaged zone but also the bentonite backfill are the main sinks for O_2, whereas corrosion of metallic components seems to play a negligible role. Previous studies estimated the duration of aerobic conditions in an emplacement drift between a few years and several decades; our results show that anaerobic conditions may be reached within a few weeks up to maximum a few months after closure of an emplacement drift for spent fuel.

1. Introduction

In a deep geological repository for radioactive waste different gaseous species will be produced, consumed and transported. Such processes can potentially affect the performance of the host rock and the engineered barrier system by changing their state conditions or by the build-up of gas pressure (Diomidis et al., 2016). In addition, such processes can affect the evolution of the repository by influencing phenomena such as porewater displacement or heat conduction.

One gaseous species that is of particular importance in the evolution of the repository near field is oxygen. Indeed, the duration of the aerobic period is a key parameter for the corrosion and lifetime prediction of spent fuel (SF) and high-level waste (HLW) disposal canisters. Furthermore, the presence of oxygen delays the generation of hydrogen due to anaerobic steel corrosion and thus controls the onset of gas production in the repository. In a HLW repository constructed in Opalinus Clay according to the Swiss disposal concept, the total amount of oxygen trapped in the near field is relatively small. Even if it was consumed exclusively by the uniform corrosion of the steel disposal canisters, it would lead to a corrosion depth smaller than 100 µm, thus contributing little to the overall corrosion allowance, which is 2 cm for the current design (Diomidis, 2014; Patel et al., 2012). However, the importance of oxygen lies on its contribution to more aggressive corrosion mechanisms such as pitting or crevice corrosion, which can endanger the integrity of the disposal canisters relatively rapidly (Landolt et al., 2009). Localized corrosion is less likely under anaerobic conditions as the thermodynamic driving force is diminished (H_2O is a less powerful oxidant than O_2) and it is less likely that the required spatial separation of anodic and cathodic processes will occur. This means that an understanding of processes affecting the fate of oxygen in a deep geological repository can simplify the description of long-term corrosion processes and mechanisms, can improve the accuracy of canister lifetime predictions and broaden the materials options under consideration for the manufacturing of disposal canisters.

Oxygen as part of free air is first introduced during excavation of the underground structures, and a continuous supply is ensured by ventilation during the operational period of the repository, which may last for decades. After backfilling and closure of the repository, oxygen remains trapped in the pore space of near field materials, where it controls the redox conditions and influences the geochemical evolution of the repository. It is expected that several processes will contribute to the consumption of O_2 after closure of the repository, leading to the eventual onset of anaerobic conditions; for instance:

- Aerobic corrosion of the numerous metallic components present in the near field of the repository, such as disposal containers and

* Corresponding author.
E-mail address: niels.giroud@nagra.ch (N. Giroud).

https://doi.org/10.1016/j.apgeochem.2018.08.011
Received 31 December 2017; Received in revised form 2 August 2018; Accepted 20 August 2018
Available online 23 August 2018
0883-2927/

tunnel support.
- Mineral oxidation: The excavation of the underground structures will expose reduced minerals, such as pyrite, to air, which will leads to their oxidation.
- Microbial activity: The repository will not be sterile, and respiration of aerobic bacteria will lead to oxygen consumption.

Predictions of the duration of the aerobic period in a HLW repository in Opalinus Clay have been based on the modelling of different oxygen consuming processes. There is significant variability in the reported results which range from a few years to several decades (Wersin et al., 2003; Landolt et al., 2009; Senger, 2015). Modelling attempts in other waste management programmes, e.g. in Canada (Kolář and King, 1996; King and Kolář, 2006) and in Sweden (Wersin et al., 1994), led to predictions of aerobic phase duration varying between a decade and several centuries. *In-situ* experiments have contributed to the exploration of the fate of oxygen in a repository in the Swiss (Giroud, 2014), French (Vinsot et al., 2014, 2017a) and Swedish (see for example Lydmark, 2011) disposal programmes. De Windt et al. (2014) modelled a fast and complete consumption of O_2 in a closed disposal cell for HLW according to the French concept, however, the materials under consideration differ significantly from the Swiss concept.

At the Mont Terri rock laboratory (Switzerland) the Full-Scale Emplacement (FE) experiment (Müller et al., 2017) provides an opportunity to study gas-related processes in-situ and at scale. As a result, the main aim of the FE-G experiment presented in this overview article is to study the various sources and sinks of gas and the associated transport processes in the FE experiment, including:

- Gas transport through the near field, excavation damaged zone (EDZ), and drift plug
- The duration of the aerobic period following backfilling
- Gas exchange with the Opalinus Clay (OPA)
- Gas-related (bio)geochemical processes

In order to deepen our understanding of these processes, a combination of field gas monitoring (Tomonaga et al., 2018 in this Special Issue), laboratory studies, and 3D reactive transport modelling is being employed. This paper describes the experimental set-ups, models and preliminary results related to the fate of oxygen.

2. Drift construction

The layout of the FE experiment was designed to simulate the Swiss repository concept for spent fuel disposal (Nagra, 2016). First, a 50-m-long experimental drift was constructed (Fig. 1). At the deep end of the FE drift a 12-m-long intermediate sealing section (ISS) was built using only steel arches and mesh for rock support, while the rest of the drift is supported by mesh and shotcrete. The shotcrete along the remaining 38 m of the drift was applied in two layers with a total thickness of at least 16 cm. The inner diameter of the FE drift varied between 2.5 and 2.7 m. The EDZ and its importance on the transport of fluids have been extensively studied, and the results are presented in Marschall et al. (2017), Lisjak et al. (2015), and references therein.

Three heaters with dimensions similar to those of SF disposal canisters were emplaced on top of bentonite block pedestals. The first heater emplaced at the deep end of the FE drift was named H1, the middle one H2, and the heater closest to the plug H3. The remaining space was backfilled with a highly compacted granulated bentonite mixture (GBM). Finally, the experiment was sealed off with a concrete plug holding the bentonite buffer in place and attempting to minimize vapour escape from the backfilled drift.

The backfilling of the FE drift was performed in several steps. The filling of the deep end of the FE drift was done in July 2014 with porous concrete. Then, a 2-m-long bentonite block wall was constructed in the ISS in early September 2014. In total, about 14 m^3 of bentonite blocks were emplaced. The average dry density of each block was 1.78 g/cm^3 and the average water content was 18 %w/w, which corresponds to an equilibrium relative humidity (RH) of approx. 70% (Garitte et al., 2015). A global bulk dry density of 1.69 ± 0.05 g/cm^3 was achieved for the entire bentonite block wall. The remaining 6.6 m of the ISS were backfilled with a total of around 70,000 kg of GBM. As preparation for each heater emplacement and backfilling, bentonite block pedestals were assembled. Heater H1 was emplaced in October 2014, heater H2 in November 2014 and heater H3 in January 2015. After the construction of each bentonite block pedestal and the subsequent emplacement of the associated heater, each section was then backfilled individually. Together with the relevant section of the ISS and the volume towards the plug, 29.6 m of the FE drift were filled with approximately 255,000 kg of GBM. The available GBM slopes were scanned with a 3D laser scanner in order to determine the backfilled volumes leading to the calculation of backfilled bulk dry density for the different sections (Fig. 2). The GBM had an initial water content of 4–6 %w/w, which corresponds to an equilibrium RH of about 50%. Overall, a global dry density of approximately 1.49 g/cm^3 was achieved. The backfilling of the FE drift was completed by stepwise construction of a vertical retaining wall in February 2015. This retaining wall consisted of 20-cm-thick concrete segments stacked in five rows. Finally, the retaining wall was sealed with two layers of resin in order to reduce vapour and gas transport. After the completion of the retaining wall, the plug was constructed. On the 17th of March 2015, 31 m^3 of self-compacting concrete were pumped into the space between the retaining wall and the formwork. Forty days after casting, the shrinkage gap at the shotcrete lining-plug interface, estimated to be less than 1 mm and resulting from settlement of the fresh concrete and from drying, was injected with resin.

3. Gas instrumentation

The bentonite backfill is equipped with sensors for the online

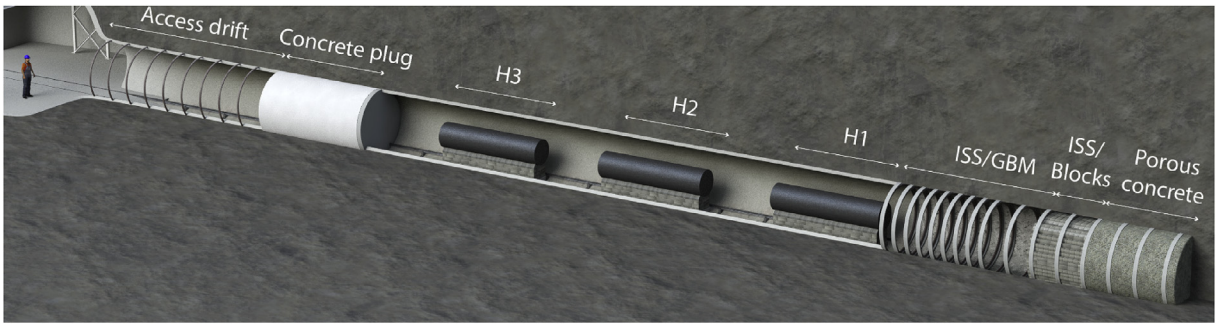

Fig. 1. Visualization of the general layout of the FE experiment and the 50-m-long FE drift. ISS: Intermediate sealing section; GBM: Granulated bentonite material; H1, H2, and H3: Heater 1, 2, and 3, respectively.

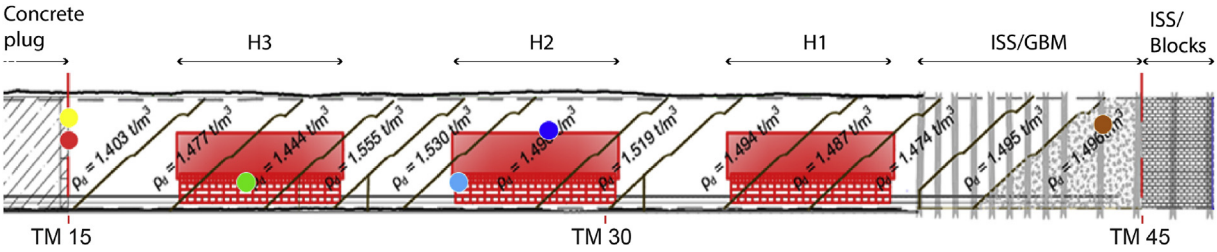

Fig. 2. Longitudinal section of the backfilled FE drift indicating the position of the 3D slope scans and the resulting bulk dry densities calculated for each of the sections. The coloured dots show the position of the O_2 sensors. The section backfilled with GBM extends between tunnel meter (TM) 15 and 45.

determination of the oxygen content of the unsaturated pore space, as well as with a series of sampling ports, distributed longitudinally and radially in the drift. The O_2 sensors, mounted in a Polyvinylidene fluoride (PVDF) housing with a silver coated Nylon filter mesh, are optical sensors of the type Hamilton® VisiFerm™ DO 120. From the total of 6 sensors, one is located in the ISS in the deepest part of the experiment, two around H2, one close to H3, and 2 on the granular bentonite side of the retaining wall (Fig. 2). The sampling ports consist of a PVDF housing of about 300 mL volume, with a coated Nylon mesh filter and two polyether ether ketone (PEEK) lines which allow the gas phase to be circulated and homogenized. Out of 10 ports, 7 have silver coated filters, and 3 are stainless steel coated. The objective of the silver coating is to limit the formation of potential biofilms and subsequent clogging of the filters. The port distribution in the drift is shown in Tomonaga et al. (2018). It should be noted that the two deepest ports are not located in the GBM like the deepest O_2 sensors, but in the porous concrete backfilling of the end of the drift. The sampling lines are connected to a gas circulation system in the access niche, allowing regular sampling of the gas phase for laboratory analysis, as well as on-line monitoring of the gas composition (e.g. N_2, O_2, He, Ar, Kr, CO_2, CH_4) by means of a quadrupole mass spectrometer (see Tomonaga et al., 2018).

4. TH evolution

An exhaustive list of the TH instrumentation and results are provided in Nagra (2018), and only the main observations are summarized here.

The heating phase started in December 2014 with H1, joined by heaters H2 and H3 in February 2015. All three heaters are power-controlled at 1350 W. The temperature is monitored in the bentonite by a total of 238 temperature sensors, as well as by ca. 300 m of fibre-optic cables (Müller et al., 2017). Additionally, boreholes drilled perpendicularly to the drift and radially around the drift from the access niche have been equipped with a total of 260 temperature sensors and 360 m of fibre-optic cable for distributed temperature sensing.

Three years after the beginning of the heating, temperatures are still increasing in the granular bentonite backfill as well as in the OPA. The temperature distribution in the granular bentonite and in the rock is a function of heater properties and heterogeneity of the thermal properties of the different materials. The heater surface temperature ranges between 117 and 133 °C. Fig. 3 shows an example of the temperatures recorded around the middle section of heater 2, at tunnel-meter (TM) 28. Temperature at the drift wall in the heated sections reaches 45–50 °C. The sensor shown in Fig. 3 (green) is located 0.8 m from the heater surface and reached 41.5 °C at the end of 2017, after about 35 months of heating. The three blue curves show sensors emplaced in a short borehole drilled into the EDZ, perpendicular to the FE drift. The shallowest sensor is located about 0.05 m into the rock (1.3 m from the heater), and the other two are 0.3 and 0.6 m deeper in the borehole, respectively. The sensor showed in violet, emplaced in a far-field borehole drilled from the access niche, shows that the temperature response to heating is slower at 2.5 m into the OPA, but the temperature

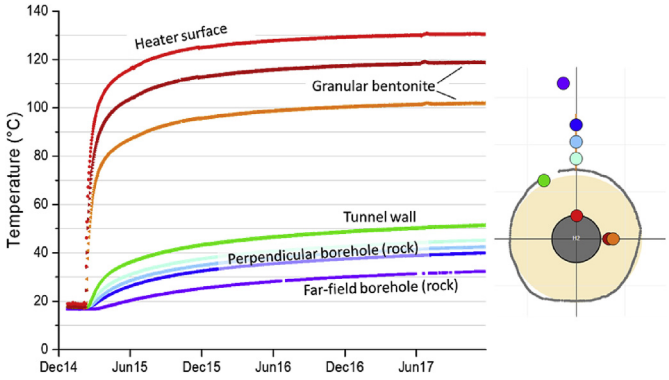

Fig. 3. Temperature evolution with time at the heater surface, in the granular bentonite and in the host rock at the section TM 28. The sketch on the right side shows the position of the selected sensors on a drift cross-section. The centre grey circle, the beige area, and the outer irregular circle represent the heater, the GBM, and the surface scan of the drift shotcrete liner, respectively. The bentonite block heater pedestal is not shown.

still increased by about 16 °C compared to pre-heating conditions.

A variety of sensors measure relative humidity (RH) and/or water content in the various parts of the experiment. In particular, the bentonite buffer is equipped with 99 RH sensors, in addition to 6 time domain reflectometry (TDR) probes (Müller et al., 2017). After backfilling of the drift and starting the heating, two competing processes affect the relative humidity in the bentonite pore space: water flowing from the host rock increases the RH of the outer periphery of the backfill, while the high temperature around the heaters dries out the bentonite and produces water flow in the gaseous form (e.g. water vapour) through the GBM, away from the heaters.

In the ISS, where the Opalinus Clay is not supported by a shotcrete liner, the EDZ has been partially desaturated due to the ventilation of the drift during the construction and emplacement phases, whereas the lined sections of the rock are close to full saturation behind the shotcrete. In the early heating phases, RH values in the range 40–50% were measured in the GBM close to the heaters, which decreased to about 20% due to heating. In the bentonite blocks, RH decreased from 80% to about 40% in the same time. In the non-heated sections only, seepage of water from the rock increases gradually the RH in the bentonite backfill. Fig. 4 shows the respective RH evolution in the EDZ (blue), at the drift wall (green), and in the GBM (orange) in the ISS, at TM 43.

5. Evolution of the O_2 concentrations in the GBM

The monitoring of O_2 in the drift backfill started during the emplacement of the experiment on 6 November 2014, when the sensors were connected to the data acquisition system. All sensors were already installed in their final position in the drift, but only the deepest one (FE_O2_080) had already been backfilled with GBM on 24 September 2014. As shown by the brown line in Fig. 5, the first measurement, 40 days after backfilling, lies below 13 %v/v O_2 and keeps decreasing to

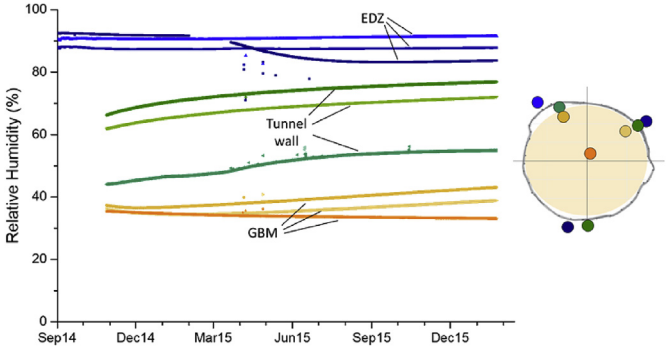

Fig. 4. Early evolution of the relative humidity at TM 43. The blue, green, and orange labels represent RH sensors located in short boreholes in the EDZ, at the drift wall, and in the GBM, respectively.

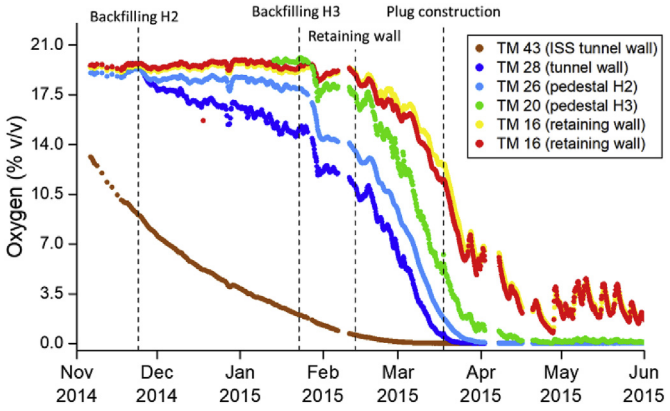

Fig. 5. Oxygen concentration in the GBM pore space atmosphere during and after backfilling and sealing of the experiment. Position of the sensors in tunnelmeters (TM), as shown in Fig. 2.

reach values below 0.1 %v/v at the beginning of March 2015, i.e. about 6 months after the sensor was backfilled. It should be noted that until the 23 October 2014, two weeks before the start of the measurements, the sensor was only distant by a few tens of cm from the open gallery. The other sensors show a rapid decrease of the O_2 concentration as soon as they are covered by GBM, as a result of competing processes of O_2 consumption, and O_2 inflow from the open gallery through the unsaturated GBM. The diffusion path length for each backfilled sensor increases at each backfilling step (slope scans on Fig. 2), resulting in a higher decrease rate until the sealing of the experiment drift with the retaining wall and the final concrete plug. The steepest slope is observed for sensors located immediately behind the retaining wall (red and yellow on Fig. 5) after completion of the plug construction. Sensors located at TM 26 and beyond (brown, dark blue and light blue) reach values below 0.1 %v/v O_2 by the end of March 2015. That corresponds to 46 days after sealing of the retaining wall with a layer of Masterseal®, and 14 days after casting of the concrete plug. The sensors located immediately behind the retaining wall do not reach the same low values and show irregular concentration variations in the range 0.5–10 %v/v. A similar behaviour is observed, although to a smaller extent, for the sensor located at TM 20 on the pedestal of heater 3. The strong variations in the measured O_2 concentrations, also observed on most other sensors during the concentration decline, are positively correlated to atmospheric pressure variations in the access niche. From this we can reasonably conclude that O_2 is transported into the FE experiment from the access niche. A few months after closing the experiment, the system approached a steady-state between inflow of O_2 and consumption. The trends observed by the in-situ sensors are confirmed by the measurements of gas species achieved by the on-line mass spectrometer (Tomonaga et al., 2018). Additionally, H_2 was detected in gas samples collected in March 2015, even before the construction of the plug, indicating that anaerobic conditions had locally been attained.

The rate of decrease in the O_2 concentration is apparently slower in the ISS than in the sections close to the heaters (Fig. 5). Consumption rates are not expected to be slower than in other sections, and the O_2 flux from the open gallery is expected to be the lowest at the deepest end of the drift. A possible explanation is that the concrete plug at the far end of the tunnel represents a large source of O_2 with limited consumption processes due to the absence of pyrite and the inhibition of corrosion and microbial processes by the alkaline pore water conditions. Therefore, O_2 from the concrete plug diffuses into the RM portion of the ISS and contributes to the apparent lower rate of consumption.

6. Laboratory tests

We conducted laboratory experiments in order to understand the role of individual materials present in the FE experiment with respect to the observed O_2 consumption. A first set of trials targeted gas dynamics in the presence of untreated FE GBM aliquots (“Mixture 3” as described in Garitte et al., 2015). The gas measurements were performed by connecting the inlet of a portable mass spectrometric system (Brennwald et al., 2016) to airtight bottles containing the material to be investigated. The same analytical system has been used for the on-line monitoring of the gas composition in the FE experiment (Tomonaga et al., 2018).

6.1. Gas measurement system

The mass spectrometric system used to measure gas species is described in detail by Brennwald et al. (2016). The system allows quantification of the partial pressures of He, Ar, Kr, N_2, O_2, CO_2, and CH_4 in gaseous and aqueous matrices with an analytical uncertainty of approximately 1–3% (standard deviation of replicate analyses of standard gas). The gas is collected through a capillary pressure reduction system into a vacuum chamber, where its composition is determined using a quadrupole mass spectrometer (Stanford Research Systems RGA-200). Calibration of the system is achieved using a gas calibration bag (Linde, Plastigas®) at an ambient pressure of approximately 960 mbar filled with atmospheric air.

The capillary inlet of the on-line gas monitoring system is connected to the outlet of a six-port selection valve (VICI® C5-2306EMHY). The inlets of the valve are connected to 1) a first stainless-steel bottle containing an aliquot of test material, 2) a second stainless steel bottle containing an additional aliquot of test material, 3) a third empty stainless-steel bottle having the same volume as the other two bottles to quantify the gas loss trough the capillary of the analytical system, 4) and a short crimped capillary for blank determination.

All stainless-steel bottles consist of a cylinder with two DN40 ends (VACOM® SC40K-316) sealed at the bottom with a blind flange (VACOM® KF40BS-316) and at the top with a DN40 to 1/4″ Swagelok® adapter (VACOM® KSWA407316). The sealing is achieved by O-rings (VACOM® KF40SVCR-316) tightened by aluminium chains (VACOM® XA40). The capillaries of the mass spectrometric system are connected to the stainless-steel bottles using 1/4″ to 1/16″ adapters (Swagelok® SS-100-R-4).

The analytical protocol starts with a calibration step followed by the determination of the analytical blank. Subsequently, gas from the three bottles is analysed at intervals of 5 h. Instrumental drifts are controlled and corrected by the analysis of gas from the calibration bag prior to the measurements of the gas from the bottles.

The data obtained from the measurement of the gas composition in the bottles containing test material are corrected for gas consumption due to the gas removal for the analyses using the according measurement of the third empty bottle.

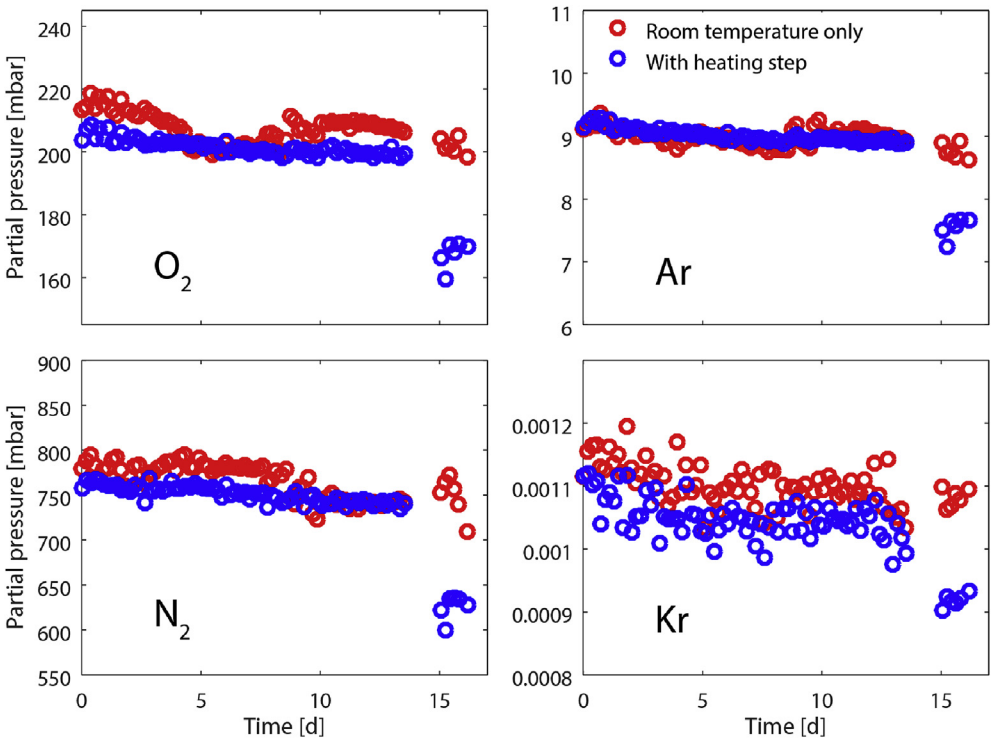

Fig. 6. Gas partial pressures determined during the measurement of the gas composition in airtight sealed bottles containing untreated bentonite. After a heating step of 1 day at 100 °C, the partial pressures of all gases in the respective bottle (blue circles) drop significantly compared to the partial pressures in the bottle kept at ambient temperature (red circles). The observation of a decrease in the partial pressure of Ar and Kr (i.e., chemically inert gas species) makes the case that bentonite can adsorb effectively gases.

6.2. Experimental results

About 15 g of granulated bentonite were filled in open glass vials which were placed into the stainless-steel bottles that were subsequently sealed airtight. The initial gas phase in the sealed bottles was atmospheric air at ambient pressure. In the experiment presented in this section all bottles were kept at laboratory temperature (~ 23 °C). The relative humidity in the laboratory atmosphere is about 55%. As the used GBM was rather dry (approximately 6 %w/w water content), the RH in the bottles is expected to not exceed this value during the measurements at ambient temperature. The experiment lasted approximately 17 days. The second bottle containing a bentonite aliquot was treated slightly differently. Starting from day 14, all the measurements were stopped, and the second bottle was heated at 100 °C for one day. From day 15 the measurements started again and were performed until day 17. Fig. 6 summarizes the results of this heated experiment.

Prior to day 14 both bottles show similar partial pressures for all measured gases. From day 15, i.e. after the 1-day-long heating of the second bottle (blue circles), the measured gas partial pressures differ significantly. The gas partial pressures in the second bottle are about 25–30% lower compared to the partial pressures of the first bottle with non-heated bentonite (red circles).

The decrease of all gas partial pressures in the second bottle makes the case that a common physical process is responsible for the observed phenomenon. As chemically inert gases such as Ar or Kr are also affected, it seems reasonable to conclude that the process responsible for the observed gas loss is gas adsorption onto bentonite. Adsorption of gases on clays has been well studied in the fields of natural gas exploration and storage, carbon storage, industrial applications (porosity measurement, chemical gas separation), as well as, in a limited manner, in the frame of radioactive waste disposal (see e.g. Gregg and Sing, 1982; Gadikota et al., 2017; Song et al., 2017; Truche et al., 2018).

However, at this stage we cannot elucidate the microscopic mechanism(s) fostering gas adsorption onto bentonite in our laboratory experiments. A potential explanation is that the 1-day-long heating step removed a share of the adsorbed water molecules from the mineral surfaces leaving free active sorption sites that were subsequently occupied by gas species.

The general trend towards slightly lower partial pressures during the first 14 days of the laboratory experiment suggests that sorption may occur also at ambient temperature. Sorption of gases on bentonite being (partly) exposed to atmospheric gases over a time span of a few years might be surprising, as the general expectation is that the sorption-effective surface area should be already saturated. Nevertheless, we cannot exclude that the storage of the bentonite (e.g., in plastic bags) was sufficient to hamper the sorption of atmospheric gases and preserve part of its sorption capacity. From the linear regression of the O_2 partial pressure data for the first 14 days we can infer a sorption rate of about $0.2 \cdot 10^{-6}$ mol/g/day. It should be noted that the gas removal necessary for each analysis in the presented experiment can partly (or completely) mask the gas consumption due to sorption. Thus, the present O_2 sorption rate should be taken as a zeroth-order estimation and gas sorption at ambient conditions should be targeted (and possibly confirmed) by future experiments. The inferred O_2 sorption rate is one order of magnitude lower compared to the range of O_2 consumption rates observed in the FE experiment (approximately $5–20 \cdot 10^{-6}$ mol/g/day). This is reasonable, as the total O_2 consumption rates neglect other processes such as chemical reactions and physical gas exchange. Thus, although at this stage we cannot fully assess the gas sorption capacity of bentonite under common environmental conditions, such process could be one of the potential O_2 sinks in the FE experiment.

7. Modelling

7.1. Reactive-transport model

The FE-G 3D reactive transport model was created using COMSOL Multiphysics® Version 5.3 and specifically the Corrosion module. A cylindrical model geometry representing the deepest part of the drift was selected for the initial development in order to avoid complications due to the expected influence of the radially varying temperature, while still maintaining the effects of the spatially and temporally varying RH (Fig. 7). Four cylindrical geometrical components were defined, comprising:

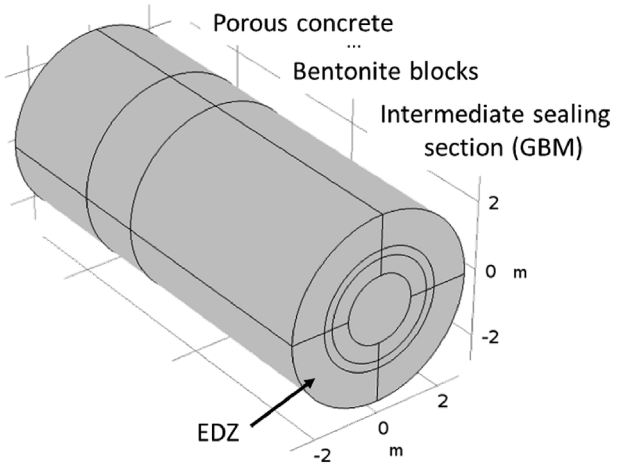

Fig. 7. Geometry of the model including the GBM, bentonite block wall, and porous concrete. The outer cylinder represents the EDZ, while the inner three nested cylinders represent the backfill with various degrees of water saturation and support steel (steel sets and steel mesh in the outer backfill cylinder).

- An inner component representing the GBM, bentonite block wall, and/or porous concrete. This cylinder of a nominal radius of 1.5 m was further divided into a central component (radius 1 m) and an outer ring (outer radius 1.5 m) to represent the different types of RH behaviour.
- An intermediate cylinder (inner radius 1.5 m and outer radius 1.75 m) representing a composite of the steel tunnel supports (steel sets and/or mesh) and either GBM or concrete.
- An outer cylinder representing the EDZ with a nominal thickness of 1 m.

In addition to the domains representing the GBM and associated steel and EDZ layers, domains were added to represent the bentonite block wall (BBW) and porous concrete and their associated EDZs, giving a total model length of 12.2 m. The model diameter, including the 1-m-thick EDZ is 5.5 m. Because of the limited number of RH sensors in the BBW and porous concrete, these domains were not further sub-divided and the RH in each was assumed to be uniform.

All components were treated as equivalent porous media with an associated porosity (φ) and tortuosity factor (τ) shown in Table 1. Some of the cylindrical components were sub-divided into upper and lower halves or into four quadrants in order to better represent the spatial variability of the RH or the positioning of steel mesh only in the upper portion of the drift. Each domain is also characterised by the time-dependent RH and the nature of the reactions occurring within the domain.

Two species were included in the model, namely gaseous (O_2(g)) and dissolved (O_2(aq)) oxygen. Dissolved O_2 is assumed to be transported, to exchange with O_2(g), and to react, whereas gaseous O_2 is assumed only to be transported or to exchange with O_2(aq). No gas-phase O_2 consumption reactions are included in the current version of the model. Dissolved and gaseous O_2 are assumed to be in equilibrium with the concentrations given by Henry's law. Transport of gaseous and dissolved O_2 is assumed to occur by diffusion only. The effective diffusion coefficient of O_2 (D_{EFF}) is a strong function of the degree of saturation (S). Equation (1) is used to describe the D_{EFF} of O_2 through unsaturated bentonite and is based on a review of gas diffusion models through unsaturated porous media by Collin and Rasmuson (1988).

$$D_{EFF} = \tau(1 - S)^3 \varphi D_A + \tau \varphi S D_0 \quad (1)$$

The two terms on the right-hand side are the contributions from O_2(g) and O_2(aq), respectively, and D_A and D_0 are the diffusion coefficients of O_2 in air and in bulk solution and have values of 0.176 cm^2/s and 2.1×10^{-5} cm^2/s at 25 °C, respectively (Cussler, 1997). This expression has been used to estimate the rate of corrosion of copper nuclear waste canisters due to the diffusion of O_2 through unsaturated bentonite buffer material (King and Kolář 1995, 2006; King et al., 2008, 2011). The RH readings from the FE probes were converted to the degree of saturation (S) using the soil-water characteristic curve (SWCC) for bentonite pellets (Man and Martino, 2009).

Oxygen is assumed to be consumed by corrosion of the steel tunnel supports and by reaction with the bentonite and OPA. In the latter cases, the exact nature of the reactions is not defined but could involve pyrite (or other oxidisable mineral phases) or aerobic microbial respiration. Finally, O_2 is assumed not to be consumed in the porous concrete (siliceous aggregate with negligible sulphide content, see Nagra, 2018). A set of six reactions are included in the model, each described by a first-order rate constant k:

- k_1 – reaction with bentonite
- k_2 – reaction with OPA in the EDZ
- k_3 – corrosion of the steel mesh in the top half of the GBM- and bentonite-block-filled sections of the ISS
- k_4 – corrosion of the steel sets encircling the entire drift in the GBM- and bentonite-block-filled sections of the ISS
- k_5 - corrosion of the steel mesh in the top half of the drift sealed by the porous concrete
- k_6 - corrosion of the steel sets encircling the entire drift around the porous concrete

Because the nature of the reactions responsible for O_2 consumption in the bentonite and EDZ are undefined, an estimated value for the respective rate constants was obtained by fitting the data from sensor FE_O2_080 to a first-order kinetic plot (Fig. 8). Clearly O_2 consumption does not follow first-order kinetics, which would be indicated by a linear kinetic plot, but the data in Fig. 8 were regardless fitted to a linear dependence to provide an estimated value for k_1 and k_2 of 4×10^{-7} s^{-1} (Table 2). The rate constants for the various corrosion

Table 1
Input parameter values used for the various materials in the model.

Material	Tortuosity factor	Porosity
GBM	1	0.44 (based on 1.49 g/cm^3 dry density)
EDZ	$\varphi^{1/3}S^{10/3}$[a]	0.137
Bentonite block (in wall)	0.1	0.33 (based on 1.78 g/cm^3 dry density)
Porous concrete	1	0.5

[a] Based on the model of Millington and Quirk (1961), where φ is porosity and S is the degree of saturation.

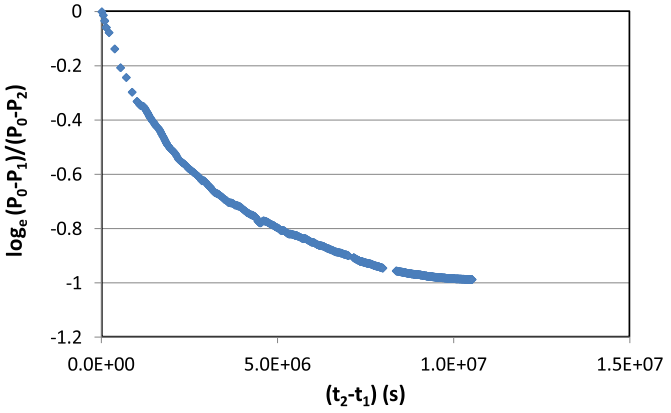

Fig. 8. First-order kinetic plot for the O_2 concentration data from sensor FE_O2_080. P_0 is the initial probe reading and P_1 and P_2 are the probe readings at times t_1 and t_2, respectively.

Table 2
Values of first-order rate constants and corresponding threshold relative humidity values.

Process	Rate constant	Value	Threshold RH
Reaction with bentonite	k_1	$4 \times 10^{-7}\ s^{-1}$	25%, 40%, 60%, 70%
Reaction with pyrite in EDZ	k_2	$4 \times 10^{-7}\ s^{-1}$	70%
Corrosion of steel mesh in GBM (top half of outer GBM layer)	k_3	$1.4 \times 10^{-8}\ s^{-1}$	70%
Corrosion of steel sets in GBM (acts on entire outer GBM layer)	k_4	$1.1 \times 10^{-7}\ s^{-1}$	70%
Corrosion of steel mesh in concrete (top half of outer concrete layer)	k_5	$1.4 \times 10^{-9}\ s^{-1}$	70%
Corrosion of steel sets in concrete (acts on entire outer concrete layer)	k_6	$1.1 \times 10^{-8}\ s^{-1}$	70%

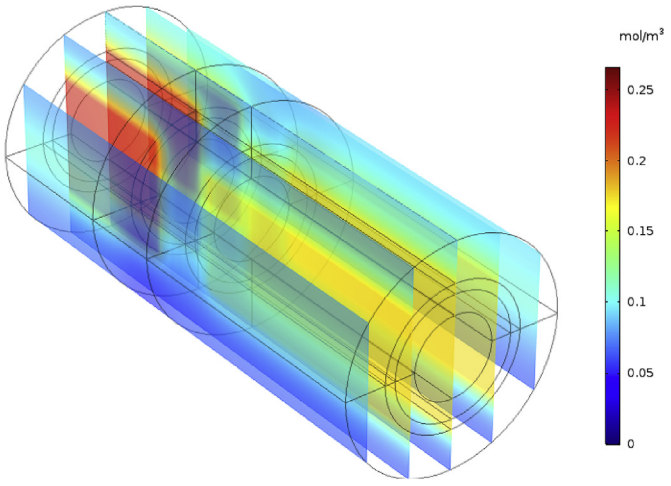

Fig. 9. Predicted distribution of dissolved O_2 at day 25 with zero-flux boundary conditions. Threshold RH for O_2 consumption by bentonite of 25%, rate enhancement factor of 25 for reaction with bentonite and the EDZ.

reactions were based on assumed aerobic corrosion rates for the steel mesh and arches in contact with bentonite of 10 µm/y and 5 µm/y, respectively, and corresponding corrosion rates for both materials in contact with the porous concrete of 1 µm/y with suitable conversion based on the respective steel surface area to bentonite or concrete volume ratios (data are available in Nagra, 2018).

Since O_2 is assumed to react in the dissolved form only, it is reasonable to expect that the reaction only occurs in the presence of sufficient moisture. This is a well-known observation in atmospheric corrosion where a threshold RH of approximately 70% is commonly observed, below which there is an insufficiently thick surface water layer for corrosion to occur. Similarly, aerobic microbial respiration would only be expected to occur at a sufficient water activity or RH (Brown, 1990). Although the RH-dependence of mineral alteration processes have been less well-studied, it does not seem unreasonable to assume that such redox reactions would also only be facilitated by the presence of liquid water. Therefore, a threshold RH was defined for each of the six reactions which, by analogy with atmospheric corrosion, was initially set to 70% for all reactions (Table 2), although this value was also varied for the consumption of O_2 by bentonite (rate constant k_1) based on preliminary experimental evidence (see Section 6 Laboratory tests).

Two different sets of boundary conditions were used. First, zero-flux conditions on all boundaries were used to allow an accurate assessment of the O_2 mass balance. Second, to better represent the expected boundary conditions within the FE experiment, a zero-flux condition was used on all surfaces except for the interface between the GBM and steel sets/mesh domains and the heated section of the drift. These latter surfaces were maintained at a constant (aerated) condition to represent the access to the atmosphere from the un-backfilled drift during the period corresponding to the decrease in O_2 concentration recorded by sensor FE_O2_080.

The focus of the modelling was an attempt to fit the observed O_2 consumption profile using a combination of enhanced rate constants and lower RH thresholds for the reaction between O_2 and bentonite. Rate enhancement factors (in this case, of 25, 50, or 100-fold) were applied to the rate of reaction between O_2 and both bentonite (rate constant k_1) and the EDZ (rate constant k_2). The rate of reaction was assumed to be the same for the GBM and the compacted bentonite in the bentonite block wall.

The threshold RH for reaction between O_2 and bentonite (rate constant k_1) was set to values of either 25%, 40%, or 60% RH. These values were selected in reference to the measured RH in the GBM (Fig. 4). At a threshold RH of 25%, the entire volume of the GBM would react with O_2. In contrast, for a threshold RH of 40%, the innermost domain of GBM would remain inactive during the period of O_2 consumption. Lastly, for a threshold of 60% RH, the bentonite within the upper-left quadrant containing the steel mesh and sets would react with O_2 whereas the bentonite associated with the steel support around the remainder of the drift would be too dry to react.

7.2. Modelling results

The model simulates O_2 transport and consumption in the entire ISS including the GBM, bentonite block wall, porous concrete, and the associated EDZs. The porous concrete is a significant source of O_2 as it is assumed to be only 50% saturated initially and because it is assumed that the oxygen does not react with the concrete itself. This source of O_2 is apparent in Fig. 9 which suggests that the interior of the porous concrete is still essentially in an aerated condition after 25 days, whereas significant O_2 consumption has already occurred in the GBM and EDZ. Since O_2 is assumed not to be consumed by the concrete, the predominant flux of oxygen is outwards towards the EDZ. This outward radial diffusion of O_2 also predominates in the GBM section of the ISS even though oxygen is consumed by the bentonite, and implies that the EDZ is the primary sink for oxygen.

The predicted rate of O_2 consumption is dependent on both the threshold RH for reaction with the bentonite and the rate of reaction in the bentonite and EDZ, as shown in the results of the sensitivity analysis presented in Fig. 10. The effect of lowering the threshold RH is to increase the volume of bentonite reacting with O_2. From a modelling perspective, we can bound the observed O_2 consumption profile either by adjusting the threshold RH to permit reaction with the entire volume of bentonite with a rate enhancement factor of 25 (green asterisk curve in Fig. 10) or by using a higher enhancement factor of 100 combined with a higher RH threshold (and, hence, a smaller volume of reacting bentonite) (red asterisk curve in Fig. 10). In both of these cases, approximately equal amounts of O_2 are predicted to be consumed in the bentonite and EDZ domains. For the low RH threshold and 25-fold rate enhancement factor, 52% of the O_2 is predicted to be consumed by reaction with the bentonite and 48% by reaction in the EDZ (for zero-flux boundary conditions). For the higher RH threshold (60% RH) and higher rate enhancement factor (x100), 44% is predicted to be consumed in the bentonite and 56% in the EDZ. In both cases $\leq 0.1\%$ of the trapped O_2 is predicted to be consumed by corrosion of the steel sets and mesh.

Further developments of the model will include the simulation of temperature-dependent processes in the heated section of the tunnel

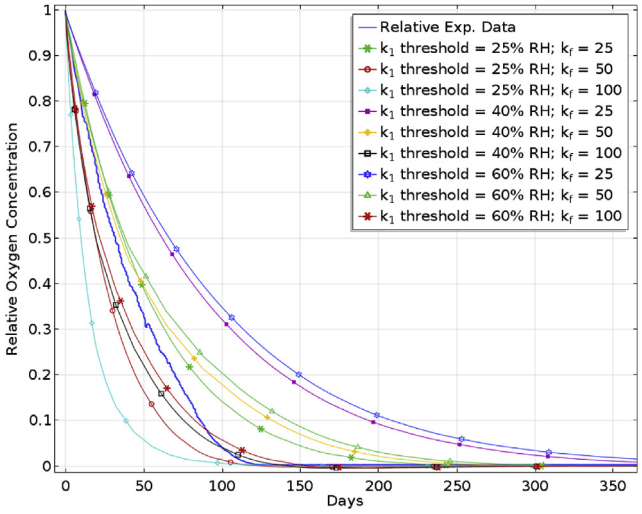

Fig. 10. Sensitivity of the time dependence of the relative O_2 concentration at the location corresponding to the sensor FE_O2_080 on the threshold RH for reaction with the bentonite and the rate enhancement factor (here denoted k_f) for reaction with the bentonite and EDZ. The time dependence of the sensor reading is also shown.

and the inclusion of possible gas-phase sorption reactions involving $O_2(g)$.

8. Discussion

The sources of O_2 in the FE experiment are the free air present in the drift during construction of the experiment, as well as air inflow. Indeed, the concentrations of O_2 near the plug clearly indicate that atmospheric air is flowing into the FE drift. The exact pathways and transport processes have not yet been studied in detail, however the correlation with atmospheric pressure points at an advective transport between the access tunnel and the backfilled drift. Most plausible pathways are instrumentation cables and pipes, the interface between the rock and the concrete plug, and the EDZ. The consequence of this inflow of O_2 on the results may be an overestimation of the O_2 concentrations in the FE experiment compared to a several hundreds of meters long SF emplacement drift.

On the other hand, the potential sinks for O_2 are:

a) Aerobic corrosion of construction material (steel mesh, steel sets, anchors, bolts) emplaced at the drift wall or in the EDZ, although corrosion rates should be lower for the elements emplaced in the high-pH shotcrete liner. The corrosion of the heaters is limited by the low relative humidity in the GBM, particularly after the beginning of the heating phase (February 2015).
b) Microbial respiration, producing CO_2; a positive CO_2 anomaly was indeed detected in one gas sampling port (Tomonaga et al., 2018), but the measured concentrations are too low to account for a significant fraction of the lost O_2, unless a significant sink would consume most of the CO_2 resulting from microbial respiration, e.g. the shotcrete and the cement backfill at the deep end of the drift. Microbial activity is also subject to the availability of water, i.e. to the periphery of the drift, as seen in Fig. 4.
c) Pyrite oxidation in the bentonite: The GBM contains about 0.3 %w/w pyrite (Garitte et al., 2015), which could mathematically account for the consumption of O_2, but the presence of water is a limiting factor for this process as well (see Equation (2)), as is the availability of fresh pyrite surfaces. The latter are, however, not realistically possible to quantify.
d) Gas exchange with the OPA porewater, as discussed in Tomonaga et al. (2018). The pyrite content of the OPA is ~ 1 %w/w (Pearson et al., 2003) and is likely to act as a sink for O_2 that dissolves into OPA porewater, most likely within the EDZ. The steady increase of light alkanes and alkenes (e.g. methane, ethane, n-/i-butane, n-/i-pentane, …), measured in the gas samples (not shown here) also confirms the presence of gas exchange processes between the FE drift and OPA porewater, as also shown by Vinsot et al. (2017b). The controlling factor for the decrease rate for this process is the dissolution rate of O_2 into the porewater, which depends on Henry's law and on the available surface area of the interface between aqueous and gaseous phases.
e) Adsorption on mineral surfaces in the bentonite: The results of the laboratory experiments tend to indicate that gas adsorption on relatively dry bentonite significantly adds to the list of O_2-consuming processes. This is consistent with the modelling results, which indicate that the inner (e.g. dryer) regions of the GBM are likely to contribute to the capture of O_2 (i.e. green asterisk curve in Fig. 10, with a lower RH threshold value of 25%). Literature data on O_2 sorption on bentonite are scarce. Volzone et al. (1999) provide equilibrium gas adsorption capacity values of montmorillonite for a variety of gases, including O_2 and N_2, but we cannot decipher adsorption rates under FE conditions with these data. Also, experimental data from the literature focus on the interaction of single gas phases with clay particles, which does not account for the competition between the gases present in the FE experiment and water (liquid and vapour). Our analyses also show that a temperature of 100 °C applied to the bentonite increases the efficiency of the sorption process. In the heated section of the FE experiment, temperatures in excess of 130 °C are measured, and this may play a significant role on the sorption properties of the bentonite. Further laboratory experiments are needed to determine temperature and RH dependency of the sorption properties of O_2 on bentonite. The adsorption of O_2 had not been considered in previous studies and may be responsible for the large overestimation of the persistence of aerobic conditions in SF and HLW emplacement drifts.

From the results of the modelling and the laboratory experiments, as well as the in-situ monitoring presented in Tomonaga et al. (2018), it seems reasonable to conclude that among the processes described above, corrosion of metals (a) and pyrite oxidation in the GBM (c) must play a negligible role in the mass balance of gaseous O_2, whereas the importance of microbial activity (b) remains unclear. The main processes controlling gases in the backfilled drift seem to be exchange with the OPA porewater (d) and sorption on GBM (e).

9. Conclusions

The fate of oxygen in a deep geological repository for spent fuel and high-level waste according to the Swiss disposal concept was studied by in-situ monitoring of a full-scale emplacement drift, bench-top experiments on individual materials and 3D reactive-transport modelling. The monitoring of the gas composition in the drift showed a rapid decrease of the O_2 concentration in the bentonite backfill, even outpacing diffusion through the granular bentonite during the backfilling process. The modelling indicates that the dominant sinks are reactions in the EDZ and in the bentonite, while corrosion of construction materials plays only a minor role in the control of O_2. However, the limited availability of water in a large section of the GBM points to the need to reconsider the interaction between bentonite and O_2. The laboratory experiments undertaken on GBM show that O_2 is being consumed by bentonite equilibrated with ~ 55% relative humidity. The fact that noble gases are captured at rates comparable to O_2 implies a sorption process on bentonite, which is consistent, at least qualitatively, with data from the literature showing an important sorption capacity of montmorillonites. Potentially, this process could even be fostered by the elevated temperatures encountered in the vicinity of the heaters in the experiment or the disposal canisters in the repository. Adsorption of

O_2 on relatively dry bentonite could at least partly explain the high consumption rates observed in the experiment, together with the exchange with the porewater of the Opalinus Clay.

Additional effort is needed to be able to quantify the different processes and their respective importance in the control of oxygen. Mineral oxidation and microbial respiration are expected to be irreversible in the boundary conditions of an underground repository, while on the other hand the reversibility of the capture of gases by sorption on bentonite minerals remains to be determined. In the case of release of O_2 from sorbing sites at a later stage, the timing and rate of release need to be better understood, in order to assess the resulting effect on the repository evolution scenarios. Complementary laboratory experiments at varying T and RH are being undertaken to address these questions, as well as the further monitoring of the in-situ experiment.

The combined results of the in-situ monitoring in the FE-G experiment, modelling and dedicated laboratory experiments indicate that anoxic conditions may be reached in an emplacement drift for spent fuel within a few weeks to a maximum of a few months after closure, which is much faster than previously estimated.

Acknowledgements

The FE experiment is part of the Mont Terri project, which is operated by Swisstopo. The FE-G experiment benefited from financial support from ANDRA (France), Nagra (Switzerland), and NWMO (Canada). The authors wish to thank the FE implementation team for making this unique experiment possible. The authors are also grateful to the anonymous reviewers for their detailed review, and for helping to improve the manuscript.

References

Brown, A.D., 1990. Microbial Water Stress Physiology. John Wiley, London.

Brennwald, M.S., Schmidt, M., Oser, J., Kipfer, R., 2016. A portable and autonomous mass spectrometric system for on-site environmental gas analysis. Environ. Sci. Technol. 50, 13455–13463. https://doi.org/10.1021/acs.est.6b03669.

Collin, M., Rasmuson, A., 1988. A comparison of gas diffusivity models for unsaturated porous media. Soil Sci. Soc. Am. J. 52, 1559–1565.

Cussler, E.L., 1997. Diffusion: Mass Transfer in Fluid Systems, second ed. Cambridge University Press, New York ISBN 0-521-45078-0.

De Windt, L., Marsal, F., Corvisier, J., Pellegrini, D., 2014. Modeling of oxygen gas diffusion and consumption during the oxic transient in a disposal cell of radioactive waste. Appl. Geochem. 41, 115–127.

Diomidis, N., 2014. Scientific Basis for the Production of Gas Due to Corrosion in a Deep Geological Repository. Nagra Working Report, NAB 14-21. Nagra, Wettingen, Switzerland.

Diomidis, N., Cloet, V., Leupin, O.X., Marschall, P., Poller, A., Stein, M., 2016. Production, Consumption and Transport of Gases in Deep Geological Repositories According to the Swiss Disposal Concept. Nagra Technical Report, NTB 16-03. Nagra, Wettingen, Switzerland.

Gadikota, G., Dazas, B., Rother, G., Cheshire, M.C., Bourg, I.C., 2017. Hydrophobic solvation of gases (CO2, CH4, H2, noble gases) in clay interlayer nanopores. J. Phys. Chem. C 121 (47), 26539–26550.

Garitte, B., Weber, H.P., Müller, H.R., 2015. Requirements, Manufacturing and QC of the Buffer Components. Nagra Working Report, NAB 15-24. Nagra Wettingen, Switzerland and EU Project LUCOEX, Deliverable D2.3. www.lucoex.eu.

Giroud, N., 2014. FEBEX – Assessment of Redox Conditions in Stage 2 before Dismantling. Nagra Working Report, NAB 14-55. Nagra, Wettingen, Switzerland.

Gregg, S.L., Sing, K.S.W., 1982. Adsorption Surface Area and Porosity, second ed. Academic Press, London, pp. 303.

King, F., Kolář, M., 2006. Simulation of the Consumption of Oxygen in Long-term In-situ Experiments and in the Third Case Study Repository Using the Copper Corrosion Model CCM-UC.1.1. Report No 06819-REP-01300-10084-R00. Ontario Power Generation, Toronto, Canada.

King, F., Kolář, M., Maak, P., 2008. Reactive-transport model for the prediction of the uniform corrosion behaviour of copper used fuel containers. J. Nucl. Mater. 379, 133–141.

King, F., Kolář, M., Vähänen, M., Lilja, C., 2011. Modelling long term corrosion behaviour of copper canisters in KBS-3 repository. Corrosion Eng. Sci. Technol. 46 (2), 217–222.

Kolář, M., King, F., 1996. Modelling the consumption of oxygen by container corrosion and reaction with Fe(II). Mater. Res. Soc. Symp. Proc. 412, 547–554.

Landolt, D., Davenport, A., Payer, J., Shoesmith, D., 2009. A Review of Materials and Corrosion Issues Regarding Canisters for Disposal of Spent Fuel and High-level Waste in Opalinus Clay. Nagra Technical Report, NTB 09-02. Nagra, Wettingen, Switzerland.

Lisjak, A., Garitte, B., Grasselli, G., Müller, H., Vietor, T., 2015. The excavation of a circular tunnel in a bedded argillaceous rock (Opalinus Clay): short-term rock mass response and FDEM numerical analysis. Tunn. Undergr. Space Technol. 45, 227–248.

Lydmark, S., 2011. SKB Project Report, P-11-16. Äspö Hard Rock Laboratory Prototype Repository Analyses of Microorganisms, Gases, and Water Chemistry in Buffer and Backfill SKB, Stockholm, Sweden.

Man, A., Martino, J.B., 2009. Thermal, Hydraulic and Mechanical Properties of Sealing Materials. Nuclear Waste Management Organization Report, NWMO TR-2009-20. NWMO, Toronto, Canada.

Marschall, P., Giger, S., De La Vaissière, R., Shao, H., Leung, H., Nussbaum, C., Trick, T., Lanyon, B., Senger, R., Lisjak, A., Alcolea, A., 2017. Hydro-mechanical evolution of the EDZ as transport path for radionuclides and gas: insights from the Mont Terri rock laboratory (Switzerland). Swiss J. Geosci. 110, 175–196.

Millington, R.J., Quirk, J.P., 1961. Permeability of porous solids. Trans. Faraday Soc. 57, 1200–1207.

Müller, H.R., Garitte, B., Vogt, T., Köhler, S., Sakaki, T., Weber, H., Spillman, T., Hertrich, M., Becker, J.K., Giroud, N., Cloet, V., Diomidis, N., Vietor, T., 2017. Implementation of the full-scale emplacement (FE) experiment at the Mont Terri rock laboratory. Swiss J. Geosci. 110, 287–306.

Nagra, 2016. Entsorgungsprogramm 2016 der Entsorgungspflichtigen. Nagra Technical Report, NTB 16-01. Nagra, Wettingen, Switzerland.

Nagra, 2018. Implementation of the Full-scale Emplacement Experiment in Mont Terri: Design, Construction and Preliminary Results. Nagra Technical Report, NTB 15-02. Nagra, Wettingen, Switzerland.

Patel, R., Punshon, C., Nicholas, J., Bastid, P., Zhou, R., Schneider, C., Bagshaw, N., Howse, D., Hutchinson, E., Asano, R., King, F., 2012. Canister Concepts for the Disposal of Spent Fuel and High-level Waste. Nagra Technical Report, NTB 12-06. Nagra, Wettingen, Switzerland.

Pearson, F.J., Arcos, D., Bath, A., Boisson, J.Y., Fernández, A.M., Gäbler, H.-E., Gaucher, E., Gautschi, A., Griffault, L., Hernán, P.W., Waber, H.N., 2003. Geochemistry of Water in the Opalinus Clay Formation at the Mont Terri Rock Laboratory. Geology Serie, No. 5. Federal Office of Topography (swisstopo), Wabern, Switzerland. http://www.mont-terri.ch.

Senger, R., 2015. Scoping Calculations in Support of the Design of the Full-scale Emplacement Experiment at the Mont Terri URL: Evaluation of the Effects and Gas Transport Phenomena. Nagra Working Report, NAB 13-98. Nagra, Wettingen, Switzerland.

Song, Y., Davy, C.A., Bertier, P., Skoczylas, F., Talandier, J., 2017. On the porosity of COx claystone by gas injection. Microporous Mesoporous Mater. 239, 272–286.

Tomonaga, Y., Giroud, N., Brennwald, M.S., Horstmann, E., Diomidis, N., Wersin, P., 2018. On-line monitoring of the gas composition in the Full-scale Emplacement experiment at Mt. Terri (Switzerland). Appl. Geochem (this issue).

Truche, L., Joubert, G., Dargent, M., Martz, P., Cathelineau, M., Rigaudier, T., Quirt, D., 2018. Clay minerals trap hydrogen in the Earth's crust: evidence from the Cigar Lake uranium deposit, Athabasca. Earth Planet Sci. Lett. 493, 186–197.

Vinsot, A., Lundy, M., Linard, Y., 2017a. O2 consumption and CO2 production at Callovian-Oxfordian rock surfaces. Procedia Earth Planet Sci. 17, 562–565.

Vinsot, A., Appelo, C.A.J., Lundy, M., Wechner, S., Cailteau-Fischbach, C., de Donato, P., Pironon, J., Lettry, Y., Lerouge, C., De Cannière, P., 2017b. Natural gas extraction and artificial gas injection experiments in Opalinus Clay, Mont Terri rock laboratory (Switzerland). Swiss J. Geosci. 110, 375–390.

Vinsot, A., Leveau, F., Bouchet, A., Arnould, A., 2014. Oxidation Front and Oxygen Transfer in the Fractured Zone Surrounding the Meuse/Haute-Marne Url Drifts in the Callovian–Oxfordian Argillaceous Rock. Geological Society, London Special Publications 400, SP400–37.

Volzone, C., Thompson, J.G., Melnitchenko, A., Ortiga, J., Palethorpe, S.R., 1999. Selective gas adsorption by amorphous clay-mineral derivatives. Clay Clay Miner. 47 (5), 647–657.

Wersin, P., Johnson, L.H., Schwyn, B., Berner, U., Curti, E., 2003. Redox Conditions in the Near Field of a Repository for SF/HLW and ILW in Opalinus Clay. Nagra Technical Report, NTB 02-13. Nagra, Wettingen, Switzerland.

Wersin, P., Spahiu, K., Bruno, J., 1994. Time Evolution of Dissolved Oxygen and Redox Conditions in a HLW Repository. SKB Technical Report 94-02. SKB, Stockholm, Sweden.